

# Scattering by atoms in zero-point states: from Debye and Waller to present days

Erik B. Karlsson\*

Department of Physics and Astronomy, Uppsala University, P. O. Box 516, SE-75120 Uppsala, Sweden.

## ABSTRACT

Ivar Waller published in 1923 a calculation of the effect of thermal vibrations of atoms on the interference in X-ray scattering. It was an extension and generalized treatment of the work by Peter Debye, first published in 1913. These two papers explained the reduction of peak intensities in X-ray diffraction. Both used the Planck distribution of oscillation frequencies based on the old quantum theory for calculating the mean square vibrational amplitudes of the scattering atoms. A zero-point residual term in the Planck formula was considered hypothetical and was neglected, but after evidence for zero-point effects had been found in the rotational energy of hydrogen molecules and Heisenberg had introduced his intrinsic uncertainties in positions and momenta, its contributions to the D-W factors were searched for in crystallographic data. With the increasing availability of low temperature scattering data in the middle of last century they were gradually observed and tabulated for atoms in different types of crystals. Scattering on hydrogen (H) represents an extreme case where zero-point motion is the dominating contribution to D-W factors. But observation of diffraction is limited both with X-rays (low coherent cross-section) and neutrons (largely incoherent due to spin-flip scattering). Therefore, its effect on H-scattering could first be studied in detail only in experiments with epithermal neutrons, starting in the 1990s. The most recent manifestation of zero-point effects is the so-called ‘hydrogen anomaly’

in Compton scattering, now understood as a reduction of neutron cross-section when it scatters on indistinguishable protons having inherent momentum uncertainties. The resulting broad distribution of scattering phases leads to a strong cross-section reduction when only a few particles are seen by each incoming neutron. The decay of the H-anomaly can be used to study chemical processes on the femtosecond scale.

**KEYWORDS:** zero-point states, neutron scattering, femtosecond phenomena.

## 1. Introduction

Zero-point motion is a genuine quantum mechanical effect without any correspondence in classical physics. Its effects have been observed in many different physical and chemical systems, in empty space as well as in atoms and molecules and it is also a main component in cosmological theories. But many of its clearest manifestations are found in scattering experiments, which will be underlined in the present article.

## 2. The zero-point motion and its manifestations

The concept of zero-point motion appeared already in the ‘old quantum theory’. Max Planck’s first formulation of the quantum theory of radiation in 1901 [1],

$$\rho(\nu) = (8\pi h\nu^3 / c^3) / (e^{h\nu/kT} - 1) \quad (1)$$

where  $\rho(\nu)$  is the density of oscillators with frequency  $\nu$ , explained excellently the “ultraviolet catastrophe” in black body radiation, but Planck was unsatisfied with the “ad hoc” assumption he

---

\*Email id: erik.karlsson@physics.uu.se

had used to derive it and explored alternative possibilities for derivation. When considering a thermodynamic model in 1912 [2] for the equilibrium of emitted and absorbed radiation he derived an expression for the energy  $U$  of an oscillator in thermal equilibrium of the form [3, eq. 223],

$$U = \frac{h\nu}{e^{h\nu/kT} - 1} \cong \frac{h\nu}{1 + h\nu/kT + \frac{1}{2}(h\nu/kT)^2 - 1} = \frac{kT}{1 + \frac{1}{2}h\nu/kT} \cong kT - \frac{1}{2}h\nu \quad (3)$$

gives the classical result  $U = kT$  only if  $U$  includes a zero-point energy  $(1/2)h\nu$ . In the same paper they showed that the temperature dependence of the specific heat of molecular hydrogen, measured by Eucken [5], could be explained by introducing a zero-point rotational energy for the molecules, in addition to the  $\Delta U = h\nu$  per angular momentum unit predicted by the ‘old’ quantum theory. This interpretation was considered by Einstein and Stern themselves as ‘highly probable’ and the agreement with experiment provided the first concrete proof of the existence of zero-point energy.

During the following hundred years, several manifestations of zero-point motion have been observed; among the ones mentioned most often are the non-freezing of liquid helium at any temperature (Simon [6] in 1934), the Lamb shift [7] between  $^2S_{1/2}$  and  $^2P_{1/2}$  energy levels in the hydrogen atom, explained in 1947, and the effect predicted by Casimir in 1948 [8] that vacuum fluctuations cause an attractive force between closely placed parallel plates, actually observed by Lamoreaux in 1997 [9]. Zero-point effects are also a basic ingredient in quantum field theories.

But larger and often much more easily accessible effects have been observed in low temperature X-ray and neutron scattering experiments, where it gives rise to a reduction of coherent scattering intensity through the Debye-Waller factors. The present note will start with a brief review of earlier observed effects of zero-point motion on scattering before describing another of its most clear and direct consequences, the scattering of epithermal neutrons on hydrogen nuclei bound in metal hydrides, where the uncertainty in the proton momentum  $n(p)$  can be mapped in detail by data from Compton scattering

$$U = \frac{1}{2}h\nu \frac{e^{-h\nu/kT} + 1}{e^{-h\nu/kT} - 1} = \frac{h\nu}{e^{h\nu/kT} - 1} + \frac{1}{2}h\nu \quad (2)$$

which in the limit  $T = 0$  contained an additional energy term  $(1/2)h\nu$ , a “zero-point energy”.

Likewise, Einstein and Stern [4] pointed out that a series expansion

experiments with neutrons (and also allows derivation of its spatial distribution  $n(x)$ ).

The latest – and perhaps most conspicuous zero-point effect – is observed in neutron Compton scattering experiments with beams covering pairs of protons or few-proton systems in dense hydrides. Here, there appears a so-called “hydrogen anomaly”: the neutron cross-sections are up to 40% lower than expected for individual protons. It has been explained as a result of destructive interference when neutrons scatter on two or more protons, each of which is distributed in space and momentum through their zero-point uncertainty [10].

### 3. Zero-point effects in scattering

#### 3.1. X-ray scattering

The notion of zero-point vibrations was mentioned, both by Debye in his first explanation of the reduction of Bragg peak intensities in X-ray scattering from vibrating particles in 1913 [11] and by Waller in his extended theory in 1923 [12]. In their calculations the atomic vibrations were expressed as ensemble averages  $\langle u^2 \rangle$  of deviations  $u$  from equilibrium positions, based on the oscillator probabilities in eq. (1). For a simple Debye model for the density of oscillator states, Debye-Waller factors for atoms on mass  $m_A$  can be expressed as  $e^{-2M}$ , where  $M = (1/2)q^2 \langle u^2 \rangle$  and

$$\langle u^2 \rangle = \frac{3\hbar^2}{m_A k\Theta} \left[ \frac{\Phi(\xi)}{\xi} + \frac{1}{4} \right] \quad (4)$$

with

$$\Phi(\xi) = \frac{1}{\xi} \int \frac{\xi}{e^{\xi} - 1} d\xi \quad (5)$$

where  $\xi = T/\Theta$ . The quantity  $\Theta$  is the Debye temperature, which reflects the strength of the force that binds the scattering atom to its crystal lattice position. In analogy with eqs. (2) and (3), eq. (4) contains the temperature-independent term  $1/4$ , a zero-point contribution with no classical counterpart. But both Debye and Waller considered - at this stage - zero-point oscillations as hypothetical and neglected them in their calculations. Therefore, the original D-W factors are equal to unity at  $T = 0$ .

With the advent of the new quantum theory the nature of zero-point motion was clarified. The relations introduced by Heisenberg and Schrödinger showed that half-values (in terms of  $\hbar$ ) must exist, both for angular momenta and for energy (in terms of  $\hbar\nu_0$ ). Particles bound by attractive potentials have a zero-point energy  $(1/2)\hbar\nu$  above the potential energy minimum and associated uncertainties  $\Delta x$  in position and  $\Delta p$  in momentum, related by Heisenberg's relation  $\Delta p \Delta x \geq \hbar/2$ .

The average squares of the position uncertainties in zero-point states add contributions  $\langle u_0^2 \rangle$  to the thermal terms  $\langle u_T^2 \rangle$  in the calculation of the Debye-Waller factors; terms that remain at zero temperature. Their magnitudes decrease with increasing mass of the scattering atoms and depend also on the stiffness of the binding potential; crystals with high Debye temperatures show higher values of  $\langle u_0^2 \rangle$ . When the scattering is described in the momentum representation, the corresponding momentum uncertainties  $\langle \Delta p_0^2 \rangle$  are the relevant quantities.

Debye-Waller factors apply to all types of coherent scattering (of X-rays, neutrons or electrons) and also to gamma-resonances in the Mössbauer effect [13]. In X-ray scattering the bound electrons in the atoms are the actual scatterers; they are supposed to follow the nuclei in their thermal vibrations (the Born-Oppenheimer approximation). The scattering electrons are distributed over the atomic volume with a radial density  $\rho(\mathbf{r})$ , as described by their wave-functions,  $\rho(\mathbf{r}) = |\Psi_{lm}^*(\mathbf{r}, \phi)\Psi_{lm}(\mathbf{r}, \phi)|$ , with a spread in position  $\Delta x$  of the order of  $0.1 - 1 \text{ \AA}$  ( $10^{-10} \text{ m}$ ). The electrons are affected by the electric field vector of the incoming photons and reradiate radiation of the same wavelength as the incident one. The scattered radiation is a spherical wave with contributions from the different volume elements of the electronic shells, having phase factors

$(\mathbf{k} - \mathbf{k}') \cdot \mathbf{r} = \mathbf{q} \cdot \mathbf{r}$  with respect to the forward scattered beam. This leads to a total scattering length  $r_0 f_Z(\mathbf{q})$  where  $r_0 = 2.82 \times 10^{-15} \text{ m}$  is the Thomson scattering length for a localized electron and  $f_Z(\mathbf{q}) = \int \rho(\mathbf{r}) \exp(i\mathbf{q} \cdot \mathbf{r}) d\mathbf{r}$  is the *atomic form factor*. For an atom of nuclear charge  $Z$ ,  $f_Z$  is equal to  $Z$  for long X-ray wavelengths but is reduced to  $f_Z < Z$  for wavelengths comparable with the electron position distribution  $\Delta x$ .

The form factor is the Fourier transform of  $\rho(\mathbf{r})$  and vice versa. When quantum mechanics had reached the point that  $\rho(\mathbf{r})$  could be obtained reliably from the atomic wavefunction  $\Psi_{lm}(\mathbf{r}, \phi)$ , James, Waller and Hartree in 1928 [14] calculated the expected  $f_Z(\mathbf{q})$  for  $\text{Cl}^-$  and  $\text{Na}^+$  ions and compared their curves (full lines in Fig. 1) with X-ray data that had been measured by James and Miss Firth [15] in 1927 on NaCl crystals at liquid nitrogen temperature. A problem was that an extrapolation to  $T = 0$  for extraction of the zero-point effect from the experimental data could not be made directly since measuring at two different temperatures does not give  $M = M(T) + M(0)$  in the D-W formula  $e^{-2M}$ , but only  $M(T_1) - M(T_2)$ . James *et al.* therefore used the existing X-ray data and their temperature factors to predict the shapes of  $f_Z(\mathbf{q})$  that should be expected if  $M(0) = 0$  (circles in Fig. 1) and with  $M(0)$  equal to the value expected with zero-point terms present (circles). The better agreement with the second hypothesis was the first evidence for zero-point effects in scattering.

More direct evidence for the zero-point effect on Debye-Waller factors at low temperature was reported by Brindley and Ridley [16] in 1938 in scattering on Mg-crystals. At  $T = 78 \text{ K}$  they observed a deviation from a proportionality to  $T$ , expected from standard thermal vibrations. Further X-ray diffraction on Mg was performed by Watanabe *et al.* [17] at  $78 \text{ K}$  and later by thermal neutrons (D. Sledziewska-Blocka and B. Lebeck [18]) down to  $5 \text{ K}$ , the latter showing a value  $\langle u^2 \rangle = 0.0130 \text{ \AA}^2$  for hexagonal Mg.

X-ray and neutron scattering data have therefore provided some of the clearest manifestations of the zero-point phenomenon. Over the last fifty years, a large body of supporting data has been collected for atoms of all sizes, placed in different kinds of crystals as exemplified in Table 1 for scattering

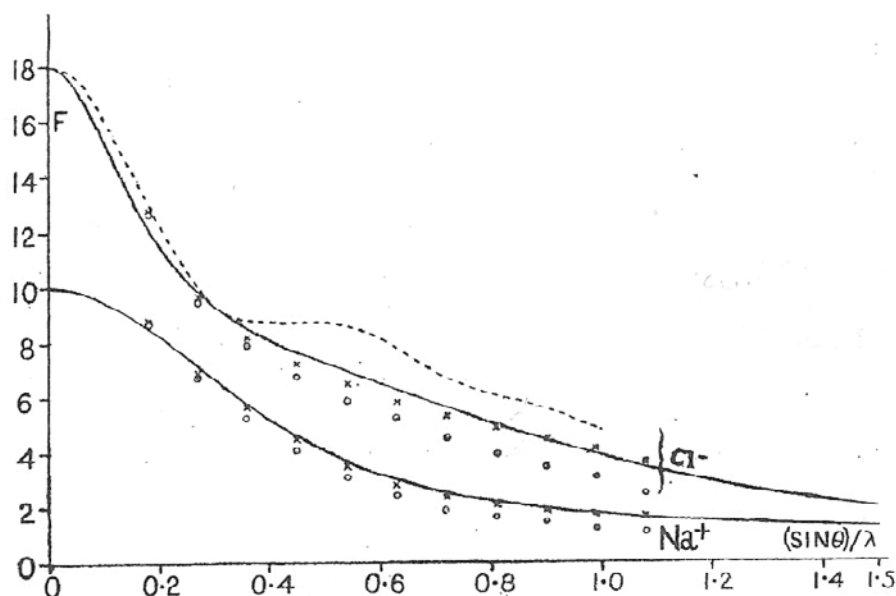


**Fig. 1.** Calculated (full lines) form factors  $F$  for  $\text{Cl}^-$  and  $\text{Na}^+$ , as compared to X-ray data taken at 78 K and extrapolated to  $T = 0$  under the assumption of zero-point oscillations (crosses) and no zero-point oscillations (circles). The transferred momentum is  $q = 4(\sin \theta)/\lambda$  (Reproduced with permission from James, R. W., Waller, I. and Hartree, D. R. 1928, Proc. Roy. Soc. A, 118, 334).

**Table 1.** Mean square amplitudes  $\langle u_0^2 \rangle$ , in units of  $\text{\AA}^2$ , Li ( $Z = 3$ ), Na ( $Z = 11$ ), K ( $Z = 19$ ) and Rb ( $Z = 37$ ) and F ( $Z = 9$ ) in fluoride crystals. Selected from [19].

Li	Na	K	Rb
0.0216	0.0194	0.0148	0.0080
F	F	F	F
0.0107	0.0126	0.0158	0.0169

on different fluoride crystals, recalculated from the tables of Gao *et al.* [19].

The zero-point effect is usually a low-temperature phenomenon only, but for C atoms in diamond its effects on coherent scattering dominates even at room temperature because of its high Debye temperature, see Yang and Kawazoe [20] (which is also an example of modern calculations of  $\langle u_0^2 \rangle$  from basic theory). With this exception, the lightest elements should be expected to show the largest zero-point effect, in particular the hydrogen isotopes. However, X-ray experiments are severely limited by the low cross-section for hydrogen atoms. Instead, the zero-point motion of hydrogen was first observed in the 1970s in experiments with neutrons,

first with quasi-elastic scattering, and more recently (from about 1990) using Compton scattering. The latest step of this development (to be described below) concerns scattering from close pairs of H- or D-isotopes which can lead to more than 40 percent reduction of scattering cross sections, even at room temperature, under the influence of the zero-point spread in position and momentum.

### 3.2. Neutron scattering

Neutrons are scattered when they come within reach of the nuclear forces from the scattering nuclei and the size of the cross section is determined by the properties of the compound nucleus formed during the interaction. The interaction range is typically of the order of  $10^{-15}$  m (similar to  $r_0$  for X-ray scattering by point-like electrons), but reaches more than  $10^{-14}$  m for the specific case of scattering on protons (scattering length  $b_H = 2.37 \times 10^{-14}$  m).

A neutron *diffraction* experiment on protons in crystalline hydrides would appear to be the ideal tool for demonstrating zero-point effects in scattering, but the coherent neutron cross-section is very small compared to the incoherent scattering caused by neutron spin-flips. However, *quasi-elastic neutron scattering* (QENS), can be measured with high

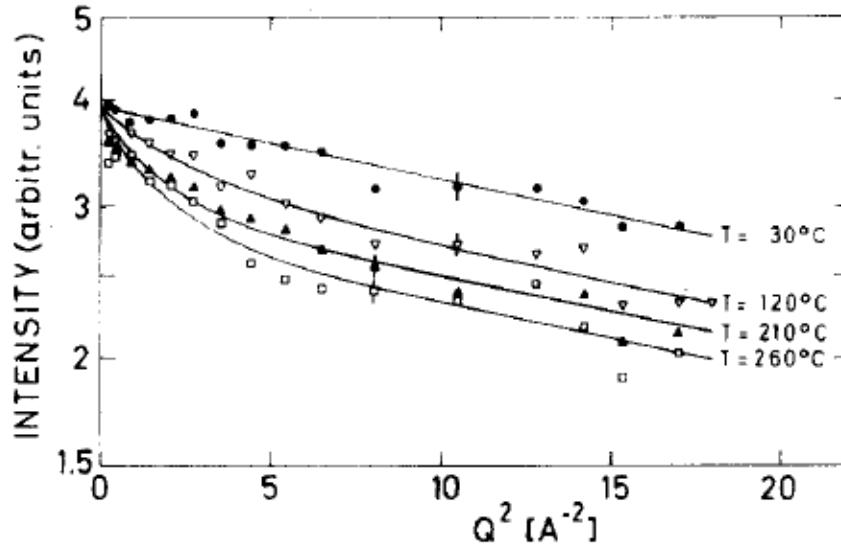


**Fig. 2.** The ordinate scale shows the intensity  $I_{QE}(q)$ , equal to the form factor squared  $|F(q)|^2$ , as function of  $q^2$  (Reproduced with permission from Wakabashi, N., Alefeld, B., Kehr, K. and Springer, T. 1974, Solid State Comm., 15, 503).

energy resolution. The scattered neutrons show a broadened peak whose reduced maximum intensity  $I_{QE}$ , depends on the scattering angle (i.e. on the transferred momentum  $q$ ). An early example is the measurement by Wakabashi *et al.* [21] from 1974 on protons in single crystals of the metal hydride  $NbH_{0.045}$  reproduced in Fig. 2. In text books, the form factor for scattering by thermal neutrons is often taken to be  $f_z \equiv 1$  because of the small nuclear size compared to the neutron wavelengths  $\lambda_{\text{thermal}}$  ( $(1-4) \times 10^{-10}$  m), but from Fig. 2 it is evident that this is not true at epithermal neutron wavelengths  $\lambda_{\text{epi}}$  ( $\approx 10^{-11}$  m) if the nuclei are in zero-point states. Then they are not localized and nuclear densities can be distributed in space with widths as large as  $\Delta x = \sqrt{\langle u_0^2 \rangle} = 2 \times 10^{-11}$  m (valid for protons in shallow crystal potentials).

Since the lowest non-zero vibrational states for the protons are excited only at about 100 meV

(i.e. at about 1000 K) the form factor data at 30 C for protons in  $NbH_{0.045}$  are related only to zero-point spreads in position. The authors' interpretation was that at 30 C the slopes corresponded to spreads in location, characterized by  $(u_0^2)_{100} = 0.038 \text{ \AA}^2$ ,  $(u_0^2)_{110} = 0.045 \text{ \AA}^2$ ,  $(u_0^2)_{111} = 0.030 \text{ \AA}^2$  along the different crystallographic axes. For the higher temperatures, the protons move by translation which causes larger broadenings.

For higher energy (so-called epithermal) neutrons in the range 5 – 100 eV, scattering is a *Compton process*, where a large fraction of energy and momentum is taken up by the recoiling nucleus. A single proton hit by a neutron recoils with a momentum  $\mathbf{q} = \mathbf{k}_0 - \mathbf{k}_1$  (which falls in the range 20 – 200  $\text{\AA}^{-1}$ ) with a recoil energy  $q^2/2m$  of several eV. The scattering function (at a temperature where only its lowest energy state is populated) is [22],

$$S(\mathbf{q}, \omega) = \sum_f \left| \int \phi_i^*(\mathbf{r}) \exp(-i\mathbf{q} \cdot \mathbf{r}) \phi_f(\mathbf{r}) d\mathbf{r} \right|^2 \delta(\hbar\omega - E_f + E_i) \quad (6)$$

In the so-called impulse approximation (IA) the recoiling proton is represented by a plane wave  $\Phi_f(\mathbf{p}') = \exp(i\mathbf{p}' \cdot \mathbf{r})$  where  $\mathbf{p}' = \mathbf{q} + \mathbf{p}$ , the sum of the recoil momentum  $\mathbf{q}$  and the momentum of the

proton in its initial state,  $\mathbf{p}$ . The interaction operator is  $O_n = b_N \exp(-i\mathbf{q} \cdot \mathbf{r})$  where  $b_N$  is the scattering length and the  $\delta$ -function ensures energy conservation with  $\hbar\omega$  the incoming neutron energy  $E_i$  and the

final state energy  $E_f = (\mathbf{p} + \mathbf{q})^2/2m$ . If the function  $\phi_i(\mathbf{r})$  is replaced by its Fourier transform  $\int \phi_i(\mathbf{p})\exp(-i\mathbf{p} \cdot \mathbf{r})d\mathbf{p}$ , the matrix element will contain the quantity  $|\phi_i(\mathbf{p})|^2 = n(\mathbf{p})$  which is the momentum probability distribution of the proton in its initial state. Converting the sum over final states to an integral the scattering function can be expressed as [22],

$$S(\mathbf{q}, \omega) = \int n(\mathbf{p})\delta[\hbar\omega - (\mathbf{p} + \mathbf{q})^2/2m + E_i]d\mathbf{p} \quad (7)$$

Therefore, when the zero-point motion dominates (as for protons bound in crystals even at room temperature) neutron Compton scattering gives a direct measure of its momentum distribution  $n(\mathbf{p})$ . The method has been used extensively for momentum distribution studies in different materials [23]; for water in confined spaces [24] the shapes of the Compton profiles have even given evidence for tunneling transfer of protons between different local potential minima.

In actual measurements, specialists express  $n(\mathbf{p})$  in terms of a scaling parameter  $y = (m/\hbar q)[\hbar\omega - q^2/2m]$ , by which measurements at different scattering angles (i.e. different  $q$ ) coalesce into a function  $J(y)$ . A typical example of zero-point momentum distributions for protons is reproduced in Fig. 3a. This measurement by Evans *et al.* [25] on the hydride  $\text{ZrH}_2$  was intended

as a control of the validity of the impulse approximation, but is actually one of the clearest demonstrations ever presented for a zero-point effect. The data in Fig. 3a are well represented by a Gaussian function  $n(\mathbf{p}) = \exp(-p^2/2\sigma_p^2)$ , as is expected if the proton is bound to a harmonic potential in the crystal. At room temperature, it could be fitted by  $\sigma_p = 4.15 \text{ \AA}^{-1}$  and measurements at 20 K gave nearly the same value. The authors noted that “the proton is effectively restricted to the ground state at both these temperatures” because the first vibrational state is excited only at 120 meV, which corresponds to 1300 K.

In an isotropic harmonic system both the variance  $\sigma_p^2$  in the momentum distribution and the variance  $\sigma_x^2$  in position are related to the normalized density of vibrational states  $Z(\nu)$  [26, 27]:

$$\sigma_p^2 = (\nu M \hbar / 2) \int \nu Z(\nu) \coth(\hbar\nu/kT) d\nu \quad (8)$$

$$\sigma_x^2 = \hbar^2 (1/2M \hbar) \int [Z(\nu)/\nu] \coth(\hbar\nu/kT) d\nu \quad (9)$$

Approximatively,  $Z(\nu)$  can be expressed as a sum of Debye density of states  $Z_D(\nu) = 3\nu^2/\nu_D$  ( $\nu < \nu_D$ ) with weight  $(1 - f)$  and a zero-point contribution  $f\delta(\nu - \nu_0)$ , where  $\nu$  is concentrated to a narrow range close to  $\nu_0$  [28]. At low temperatures, eqs. (8) and (9) reduce to

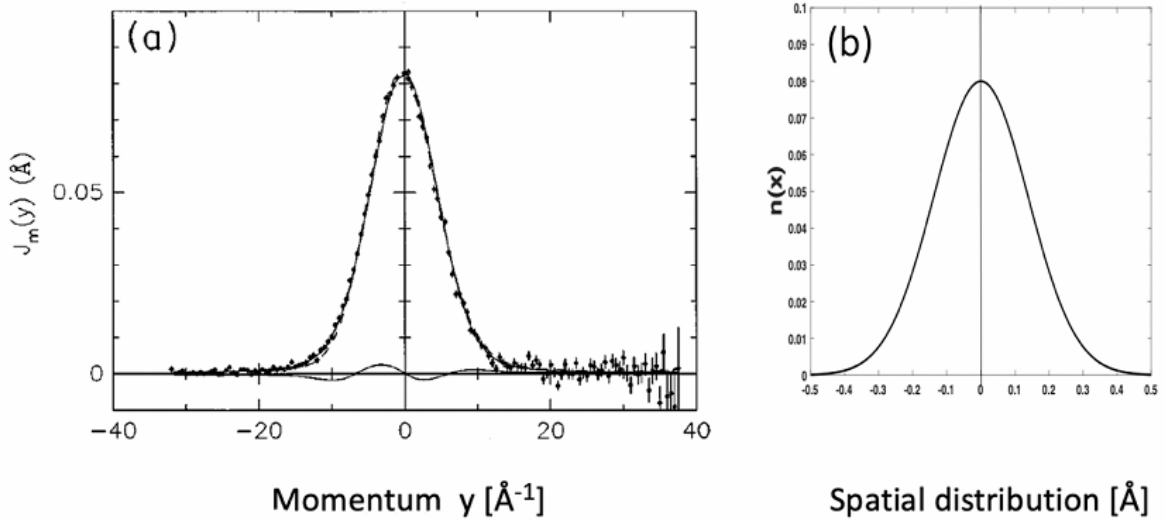


**Fig. 3.** (a) Momentum distribution for protons in the metallic hydride  $\text{ZrH}_2$ . Here,  $J_m(y)$  is an integral corresponding to the momentum distribution  $n(\mathbf{p})$  and  $y = (m/\hbar q)[\hbar\omega - q^2/2m]$  (Reproduced with permission from Evans, A. C., Timms, D. N., Mayers, J. and Bennington, S. M. 1996, Phys. Rev. B, 53, 3023); (b) Corresponding spatial distribution of H-density).

$$\sigma_p^2 = (1-f)(3M\hbar v_D/8) + f(M\hbar v_0/2) \quad (10)$$

$$\sigma_x^2 = \hbar^2[(1-f)(3/4M\hbar v_D) + f(1/2M\hbar v_D)] \quad (11)$$

Since  $f=1$  is a good approximation for protons in a metallic lattice at room temperature,  $\sigma_x^2$  and  $\sigma_p^2$  are related by  $\sigma_x^2\sigma_p^2 = \hbar^2/4$ , which is recognized as the well-known Heisenberg relation  $\sigma_x\sigma_p = \hbar/2$  for the widths of spatial and momentum distributions. The spatial density distribution  $n(x) = \exp(-x^2/2\sigma_x^2)$ , corresponding to  $n(p)$  of Fig. 3a is plotted in Fig. 3b. Its variance  $(\sigma_x)^2$ , which is equivalent to  $\langle u_0^2 \rangle$ , is  $0.038 \text{ \AA}^2$ , similar to the value found for H in in  $\text{NbH}_{0.045}$  [21].

### 3.3. Comparison of zero-point effects in X-ray and neutron scattering data

Before considering the most recently observed zero-point effect to be described below, it is appropriate to consider the time scales of X-ray and neutron scattering. A sharp Bragg pattern in X-ray or neutron diffraction requires scattering from at least  $N \approx 100$  atoms or nuclei exposed to the infalling beam. With a velocity of  $3 \times 10^8 \text{ s}$  for X-rays and  $2 \times 10^3 \text{ m/s}$  for thermal neutrons the duration of the scattering process for systems of that size is about  $10^{-16} \text{ s}$  for X-rays and  $10^{-12} \text{ s}$  for neutrons. It is noted that thermal vibration periods for atoms normally fall in the range  $10^{-13} \text{ s}$ , but for the

lightest atoms (like hydrogen bound in crystals) they are about 10 times shorter,  $10^{-14} \text{ s}$ . As far as the effect of thermal vibrations is concerned, standard X-ray diffraction would register an ensemble average of atoms in different vibrational phases, whereas neutron diffraction also sees a time average of the vibrational amplitudes (squared).

Registration of scattering events involving one or a few particles, as in quasi-elastic neutron scattering and Compton scattering of neutrons (now also observable in X-ray-FEL experiments) is a faster process, involving times below  $10^{-15} \text{ s}$  for the 1 – 100 eV neutrons used in Compton scattering. Each single event in Compton scattering sees the thermal vibration of the scattering proton in a particular vibrational phase, which is schematically illustrated in Fig. 4.

For zero-point states the scattering is fundamentally different. The spread of the particle's wavefunction has no time structure; the atom with its nucleus is quantum delocalized and there is an intrinsic uncertainty in momentum represented by the distribution  $n(p)$ . Phase shift effects in scattering from pairs of atoms in zero-point states must be integrated over the whole phase space, even when the scattering time is shorter than the period of oscillation for thermal vibrations. In Fig. 4 it is assumed that the protons are confined to a

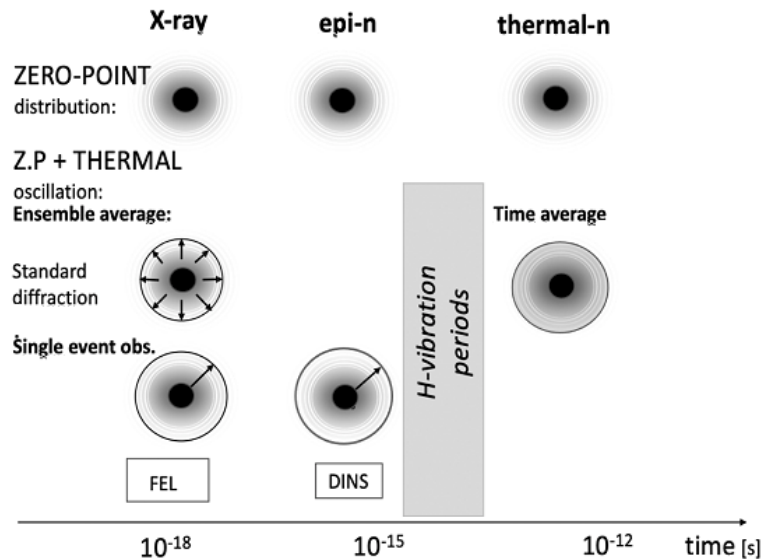


**Fig. 4.** Schematic illustration of conditions for scattering. For hydrogen, thermal excitation is important only above 1000 K.

harmonic potential where their low temperature probability density and momentum distribution has a 3D Gaussian form. Thermal excitation adds  $\langle u_T^2 \rangle$  to  $\langle u_0^2 \rangle$ .

### 3.4. Reduced cross-sections for scattering on quantum correlated proton pairs

The instrument eVS (now modified and renamed “VESUVIO”) at ISIS, Rutherford-Appleton Laboratory, UK is a so-called inverted spectrometer, where a “white spectrum” of neutrons hits the target and energy selection is performed by a resonance foil in the outgoing neutron beam. In a time-of-flight spectrum for the outgoing neutrons, the neutron hits the detector after a time  $L/v_0$  (spent from the clock start up to the target) plus  $l/v_1$  (from the target nucleus to the detector). The velocity of the outgoing neutron is the vector sum  $\mathbf{v}_1 + \mathbf{v}_p$  where  $\mathbf{v}_1$  is determined by the collision with the target mass  $M$  (for  $M = m$ ,  $v_1 = v_0 \cos \theta$  where  $\theta$  is the scattering angle), and  $\mathbf{v}_p = \mathbf{p}/M$ , where  $\mathbf{p}$  is the momentum of the target nucleus at the time of scattering. For one single type of nuclei (with mass  $M$ ) the ToF spectrum contains a Compton peak with a width characterized by  $\sigma_p$ , centered at a specific time for each scattering angle, determined by the kinematic equations,

$$\frac{v_1}{v_0} = \frac{\cos \theta + \sqrt{(M/m)^2 - \sin^2 \theta}}{(M/m) + 1} \quad (12.a)$$

$$t = \frac{L}{v_0} + \frac{l}{v_1} \quad (12.b)$$

The momentum distribution illustrated in Fig. 4 was obtained by this method. When neutrons Compton-scatter from more than one type of nuclei in a target, each of them shows a characteristic Compton peak at a specific position in the ToF spectrum. Fig. 5 is an example from the work of Karlsson *et al.* [29] concerning the mixed hydride  $\text{NbH}_{0.16}\text{D}_{0.70}$  at a neutron scattering angle of 65 degrees. It was measured on a self-supporting hydride foil (i.e. with no container background). Momentum distributions can be derived for each of the constituents, Nb, H and D, and also their relative intensities, which are represented by the content in their respective Compton peaks.

The purpose of the experiment on this metallic hydride was to verify the result of a previous neutron Compton scattering study by Chatzidimitriou-Dreismann *et al.* [30] on water which showed that the relative H/D intensity ratios in isotope mixed water,  $\text{H}_x\text{D}_{2-x}\text{O}$  fell around  $I(\text{H})/I(\text{D}) = 8.0$  instead of the expected ratio  $\sigma_{\text{H}}/\sigma_{\text{D}} = 81.9/6.25 = 13.1$ , where  $\sigma_{\text{H}}$  and  $\sigma_{\text{D}}$  are the tabulated neutron cross sections for protons and deuterons, respectively. The  $\text{NbH}_{0.16}\text{D}_{0.70}$  hydride experiment verified this anomaly and showed also that not only H/D-ratios, but also H/Nb and D/Nb peak ratios were reduced with respect to expectations, a phenomenon which became known as the “hydrogen anomaly” in neutron scattering [10]. For the highest scattering angles the H/Nb anomaly amounted to as much as 40%. In the same measurement it was also observed for the first time that the H-anomaly was larger for higher scattering angles (higher  $q$ -transfer) than for lower angles. Measurement at 20 K gave the same result as at 300 K, with respect to relative intensities as well as scattering angle dependence (ref. [29], Fig. 6). A more extensive study of hydrogen anomalies was later made in Yttrium hydrides (Karlsson *et al.* (2017) [31]), from which Fig. 6 below is extracted. The normalized H-cross sections in the plots are derived from measured ratios  $\sigma_{\text{H}}/\sigma_{\text{Y}}$  where the heavy element is taken to be independent of the quantum correlations important for protons and deuterons. It was checked in separate experiments that the “missing intensity” was not found below the Compton peak or as a diffuse background in the time-of-flight spectra.

Again, the H-anomaly amounts to about 40% at the highest scattering angles. The angular dependence (upper curve in Fig. 6) can be transformed to a scattering time dependence (lower curve) since there exists a relation [32] between  $\tau_{\text{sc}}$  and the transferred angular momentum  $q$  ( $= q_1 \tan \theta$  for protons;  $q_1 = 48.6 \text{ \AA}^{-1}$ , with Au-197 resonance foil selection of outgoing neutron energy),

$$\tau_{\text{sc}} = m_p \hbar / q_1 \tan \theta \sqrt{\langle p^2 \rangle} \quad (13)$$

Scattering times fall in the range  $(0.3 - 2) \times 10^{-15} \text{ s}$  at the scattering angles chosen.

The theoretical description of scattering on identical particles in zero-point states was developed in the period 2000–2018 [33, 34], as summarized in the review [10] mentioned above. The basic steps are reproduced below.

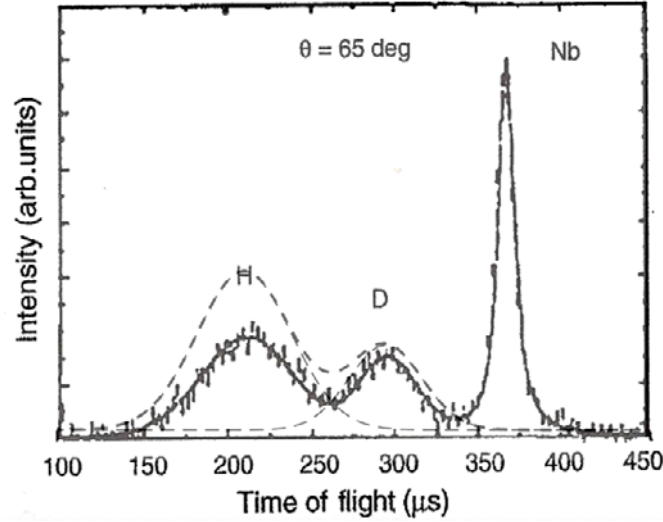


**Fig. 5.** Time-of flight spectrum for neutrons, with recoil peaks with scattering on H and D and Nb in  $\text{NbH}_{0.16}\text{D}_{0.70}$ . The experimental peak areas for H and D (Reproduced with permission from Karlsson, E. B., Chatzidimitriou-Dreismann, C. A., Abdul-Redah, T., Streffer, R. M. F., Hjørvarsson, B., Öhrmalm, J. and Myers, J. 1999, *Europhys. Lett.*, 46, 617) are reduced compared to what should be expected for the actual concentrations (dashed lines).

### 3.5. Coherence in scattering on pairs of particles in zero-point states

It took more than a decade before the hydrogen anomalies could be properly explained. In a first attempt by Karlsson and Lovesey in 2000 [33] it was pointed out that if each neutron interacts with two equivalent protons it sees these two particles as indistinguishable and anti-symmetrization rules apply, which results in an entanglement of their spin and orbital wave-functions. Such interactions can appear even at eV energies (although neutron wavelengths are smaller than typical distances between nuclei) because neutron *coherence lengths* still allow overlap of the neutron wave with two or more protons if the energy selection is sharp enough and detector solid angles are small. If the neutron scatters on two protons only, the initial state seen by the neutron must be expressed as

$$\Psi_i = (1/\sqrt{2})\{\varphi(\mathbf{R}_{a1})\varphi(\mathbf{R}_{b2}) + (-1)^J \varphi(\mathbf{R}_{b1})\varphi(\mathbf{R}_{a2})\} \chi_M^J(a, b) \quad (14)$$

with particle  $a$  having equal amplitudes at sites  $\mathbf{R}_{a1}$  and  $\mathbf{R}_{a2}$  and similarly for particle  $b$ . The spins  $I_a$  and  $I_b$  of the two particles add up to quantum numbers  $J$  and  $M$ , described by the spin function  $\chi_M^J(a, b)$ . The result of the neutron interaction is

that one of the particles recoils with momentum  $\mathbf{p}' = \mathbf{q} + \mathbf{p}$ , where  $\mathbf{p}$  is the zero-point momentum in its position in the molecule or crystal.

In the final state, described by  $\Psi_{f,\text{Compt}}$ , one of the two particles (could be  $\alpha$  or  $\beta$ ) takes up the recoil and is expelled in the form of a plane wave, while the other one ( $\beta$  or  $\alpha$ ) remains at its site. The first theoretical paper [33] on neutron scattering on indistinguishable particles was incomplete in the treatment of the final neutron state; a mistake that was corrected by Karlsson in 2012 [34]. The exchange symmetry requires that the final state wavefunction is represented by two interfering waves  $\Psi_{f,\text{Compt}}(1)$  and  $\Psi_{f,\text{Compt}}(2)$  with opposite phase factors [10, 34].

$$\begin{aligned} \Psi_{f,\text{Compt}}(1) &= \\ &= (1/2\sqrt{2})\{\exp(i\mathbf{p}' \cdot \mathbf{R}_{a1})\varphi(\mathbf{R}_{b2}) + (-1)^J \exp(i\mathbf{p}' \cdot \mathbf{R}_{a2})\varphi(\mathbf{R}_{b1}) + \\ &+ \varphi(\mathbf{R}_{a1})\exp(i\mathbf{p}' \cdot \mathbf{R}_{b2}) + (-1)^J \varphi(\mathbf{R}_{a2})\exp(i\mathbf{p}' \cdot \mathbf{R}_{b1})\} \chi_M^J(a, b) \end{aligned} \quad (15.a)$$

$$\begin{aligned} \Psi_{f,\text{Compt}}(2) &= \\ &= (1/2\sqrt{2})\{\exp(i\mathbf{p}' \cdot \mathbf{R}_{a1})\varphi(\mathbf{R}_{b2}) - (-1)^J \exp(i\mathbf{p}' \cdot \mathbf{R}_{a2})\varphi(\mathbf{R}_{b1}) + \\ &+ \varphi(\mathbf{R}_{a1})\exp(i\mathbf{p}' \cdot \mathbf{R}_{b2}) - (-1)^J \varphi(\mathbf{R}_{a2})\exp(i\mathbf{p}' \cdot \mathbf{R}_{b1})\} \chi_M^J(a, b) \end{aligned} \quad (15.b)$$

where  $\exp(i\mathbf{p}' \cdot \mathbf{R}_{a1})$  is a plane wave representing the proton expelled in the Compton process

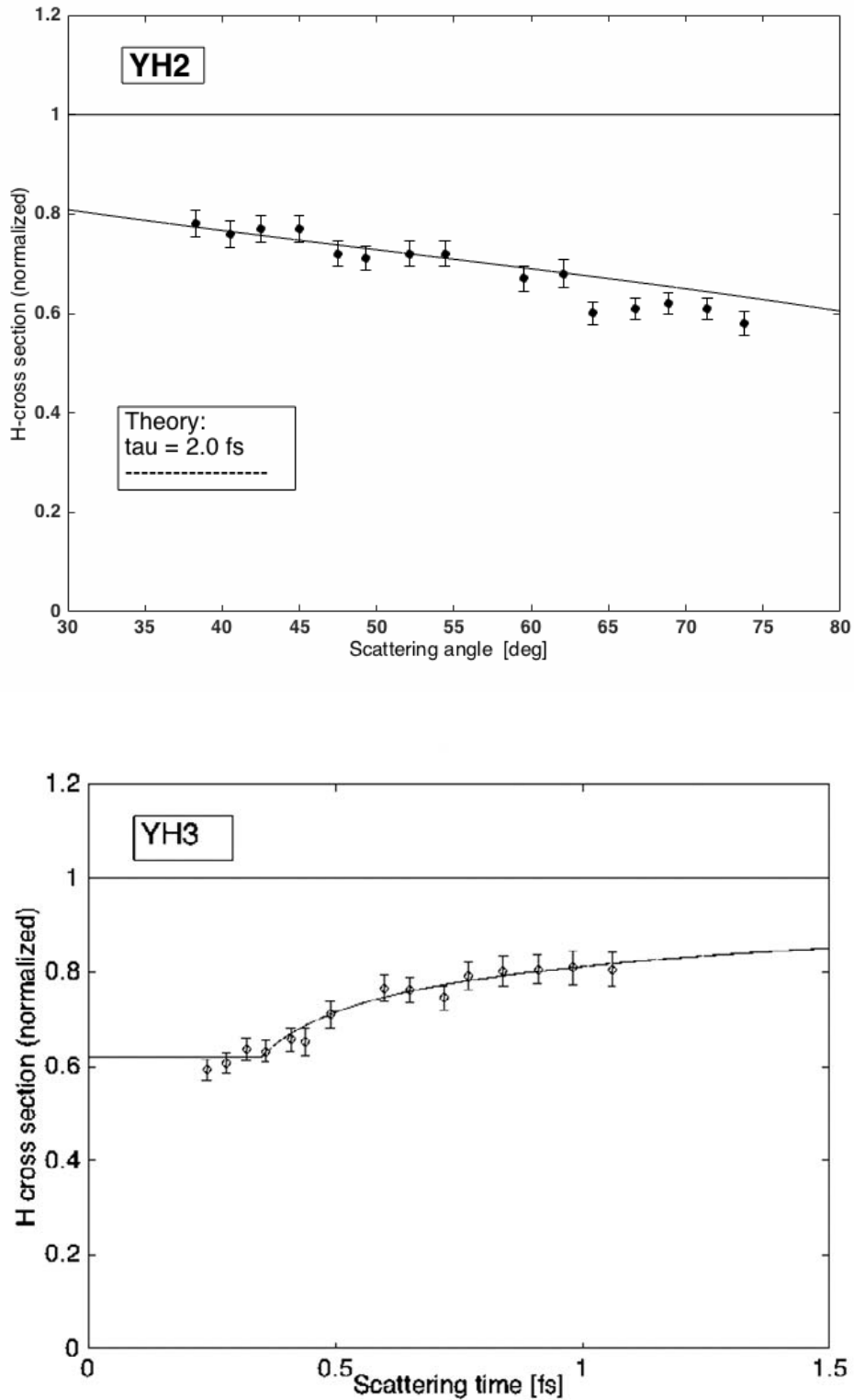


**Fig. 6.** Hydrogen anomaly ( $\sigma_{\text{obs}}/\sigma_{\text{tab}}$ ) in Compton scattering of H in Yttrium hydrides (Reproduced with permission from Karlsson, E. B., Hartmann, O., Chatzidimitriou-Dreisemann, C. A. and Abdul-Redah, T. 2016, *Meas. Sci. Technol.*, 27, 085501). Upper panel: scattering angle dependence. Lower panel: scattering time dependence.

(cf. text below eq. (6)) and  $\varphi(\mathbf{R}_{b2})$  the one remaining on the initial site, etc.

A standard calculation [34] of the spatial part of

scattering matrix elements with the neutron-proton interaction in the form  $O_n = b_n[\exp(i \mathbf{q} \cdot \mathbf{R}_a) + \exp(i \mathbf{q} \cdot \mathbf{R}_b)]$  leads to

$$\langle \Psi_{f, \text{Compt}}(1) | O_n | \Psi_i \rangle_{\text{spat}} = (1/4) \{1 + (-1)^{l+l'} \exp(i \mathbf{p} \cdot \mathbf{d})\} K(\mathbf{p}) \quad (16.a)$$

$$\langle \Psi_{f, \text{Compt}}(2) | O_n | \Psi_i \rangle_{\text{spat}} = (1/4) \{1 - (-1)^{l+l'} \exp(i \mathbf{p} \cdot \mathbf{d})\} K(\mathbf{p}) \quad (16.b)$$

where  $\mathbf{d} = \mathbf{R}_1 - \mathbf{R}_2$  and  $K(\mathbf{p})$  is the Compton integral  $K(\mathbf{p}) = \int d\mathbf{R} \exp(-i \mathbf{p} \cdot \mathbf{d}) \phi(\mathbf{R})$  mentioned earlier.

The result is a modified cross section per nucleus as compared to single particle scattering  $\sigma_{\text{sp}}$ ,

$$\begin{aligned} \sigma_{\text{eff}} &= (1/4) \{ [1 + \langle \exp(i \mathbf{p} \cdot \mathbf{d}) \rangle]^2 + [1 - \langle \exp(i \mathbf{p} \cdot \mathbf{d}) \rangle]^2 \} \sigma_{\text{sp}} \\ &= (1/2) (1 + \langle \exp(i \mathbf{p} \cdot \mathbf{d}) \rangle^2) \sigma_{\text{sp}} \end{aligned} \quad (17)$$

For a particle at rest,  $\mathbf{p} = 0$  and the scattering cross-section (per particle) is  $\sigma_{\text{eff}} = \sigma_{\text{sp}}$ . For particles in *thermal vibration* [the Debye fraction  $(1 - f)$  in eq. (9)] each scattering event has a  $\mathbf{p} \cdot \mathbf{d} = p_v d \cos\theta$  factor, where  $p_v = (3/8)Mh\nu_D$ . Averaging  $\langle \exp(ip_v d \cos\theta) \rangle^2$  over  $\theta$  with  $\nu_D \approx 10^{14} \text{ s}^{-1}$  (valid for scattering on protons) over a set of Compton scattering events gives reductions in  $\sigma_{\text{eff}}$  of the same order of magnitude as typical D-W factors.

Scattering on *zero-point states* (the  $f$ -fraction) is fundamentally different since the protons are simultaneously in all motional states allowed by the  $n(\mathbf{p})$  distribution (cf. Fig. 4). For each scattering event the factor  $\langle \exp(i \mathbf{p} \cdot \mathbf{d}) \rangle^2$  must be integrated over the  $n(\mathbf{p})$  distribution,

$$\langle \exp(i \mathbf{p} \cdot \mathbf{d}) \rangle = \int n(\mathbf{p}) \exp(i \mathbf{p} \cdot \mathbf{d}) d\mathbf{p} \quad (18)$$

For  $\mathbf{p} \perp \mathbf{d}$  eq. (17) gives the standard result  $\sigma_{\text{eff}} = \sigma_{\text{sp}}$ , but for  $\mathbf{p} \parallel \mathbf{d}$  the integral in eq. (18) is strongly reduced when the distribution  $n(\mathbf{p})$  contains several oscillations in the exponential. For H in metallic hydrides with typical  $n(\mathbf{p})$  widths  $\sigma_p = 4 \text{ \AA}^{-1}$  and H-H distances  $d = 2.5 \text{ \AA}$ , the  $\mathbf{p} \parallel \mathbf{d}$  integral is effectively zero, which leads to a reduction  $\sigma_{\text{eff}} = (5/8)\sigma_{\text{sp}}$  in eq. (17). A more refined calculation, which can be found in ref. [31], resulted in  $\sigma_{\text{eff}} = 0.56\sigma_{\text{sp}}$  for the actual scattering conditions on the Y-hydrides.

The large hydrogen anomalies of 30 – 40% observed in neutron Compton scattering on hydrogen are therefore effects of zero-point motion (also supported by the T-independence of the data in the 20 – 300 K range for hydrogen [29]). In physical terms, the cross-section reduction is caused by destructive interference when partial waves with a phase distribution covering a large fraction of  $2\pi$  are scattered from the two centers.

In Fig. 6 the H cross-section reduction reaches about  $\sigma_{\text{eff}} = 0.6 \sigma_{\text{sp}}$  at the highest scattering angles measured in the Y-hydride experiment. Remembering eq. (13), this corresponds to the lowest sampling time (about  $3 \times 10^{-16} \text{ s}$ ) where the entanglement can still be taken to be unperturbed by external interactions. At smaller scattering angles (corresponding to longer scattering times) the entanglement is reduced through decoherence by interaction with the environment (decoherence time  $\tau_{\text{coh}}$ ), resulting in a smaller H cross-section reduction. In the long-time limit, phase memory is lost and single particle scattering is expected.

Without decoherence the probability for scattering at time  $t$  is  $e^{-t/\tau_{\text{sc}}}$ , but an environment-induced decoherence  $e^{-t/\tau_{\text{coh}}}$  leads to a joint probability for observing a cross section reduction at time  $t$  as  $e^{-t/\Lambda}$ , where  $\Lambda = \tau_{\text{sc}} \tau_{\text{coh}} / (\tau_{\text{sc}} + \tau_{\text{coh}})$ . Based on these relations and using eq. (13), an explicit relation for the  $\theta$ -dependence of  $\sigma_{\text{eff}}$  was derived in ref. [31], with  $K$  a known instrumental constant,

$$\frac{\sigma_{\text{eff}}(\theta)}{\sigma_{\text{sp}}} = 1 - \frac{(3/8)}{1 + K/48.6 \times \tan \theta \times \tau_{\text{coh}}} \quad (19)$$

The line in Fig. 6a was a fit to the experimental data with  $\tau_{\text{coh}}$  as the only free parameter. The fitted value,  $\tau_{\text{coh}} = 2.0$  fs, was close to what can be expected from decoherence induced by conduction electrons which reduces the spatial and spin entanglement in a metallic hydride [30]. A more detailed analysis of the high-angle data (corresponding to the shortest observation times) indicates a plateau, within which decoherence has not yet had time to act (Fig. 6, lower panel). Here the recoiling particle is still within the amplitude range  $\Delta x \approx \hbar/\Delta p \approx 0.2$  Å of the zero-point vibration and has not yet been influenced by the intra-atomic environment [10, 31].

### 3.6. Influence of fluctuating H-bonds in water

Hydrogen bonds in water are known to fluctuate with rates from  $10^{13}$  to  $10^{14}$  s<sup>-1</sup>. Neutron Compton scattering experiments on water at room temperature were performed by Mayers and Abdul-Redah [35]

and analyzed by Karlsson [10]. A fit to eq. (19) resulted in a decoherence time of  $\tau_{\text{coh}} = 13 \pm 2$  fs, i.e. essentially longer than in the conduction electron-induced effect in the metal hydride. The main perturbation in water is through fluctuating H-bonds. The entangled wavefunction (eq. (14)) of the protons is coupled to the molecular vibrations, which are of stretching  $\mathbf{p}_s$  or bending  $\mathbf{p}_b$  type with frequency  $\omega$ , themselves coupled by hydrogen bonds to the nearest surrounding H<sub>2</sub>O molecules (Fig. 7).

During the vibrations, quantum phase relations between the proton wave functions will still remain as long as they are not perturbed by fluctuating surroundings. However when the vibrations are modified to  $\omega + \omega_{\sigma 1}$  and  $\omega + \omega_{\sigma 2}$ , there will enter time-dependent terms  $\exp[i\{\varphi + (\omega_{\sigma 2} - \omega_{\sigma 1})t\}]$  in the matrix elements  $\exp(i\mathbf{p} \cdot \mathbf{d})$  of eq. (16). In ref. [36] the mean value of the phase factor multiplying the matrix element  $\langle \exp(i\mathbf{p} \cdot \mathbf{d}) \rangle$ , was calculated as

$$\frac{1}{\sigma_{\omega} \sqrt{\pi}} \int d\omega_{\sigma} \exp[-(\omega_{\sigma} - \omega_{\sigma 0})^2 / 4\sigma_{\omega}^2] \exp(i\omega_{\sigma} t) = \frac{1}{\sigma_{\omega} \sqrt{\pi}} \int \exp[-\sigma_{\omega}^2 t^2] \exp(i\omega_{\sigma} t) \quad (20)$$

where the decay factor  $\exp[-\sigma_{\omega}^2 t^2]$  measures the decoherence. This function relates the decoherence rate in Compton scattering to the vibrational spectroscopy data. The fluctuation rate  $\sigma_{\omega} = 1/\tau_{\text{coh}} = 0.7 \times 10^{14}$  s<sup>-1</sup> derived from the

Compton scattering data agrees well with vibrational spectroscopy data by Bratos *et al.* [37], which showed an energy spread of 0.03 eV in the 0.46 eV state corresponding to  $\sigma_{\omega} = 0.5 \times 10^{14}$  s<sup>-1</sup>.

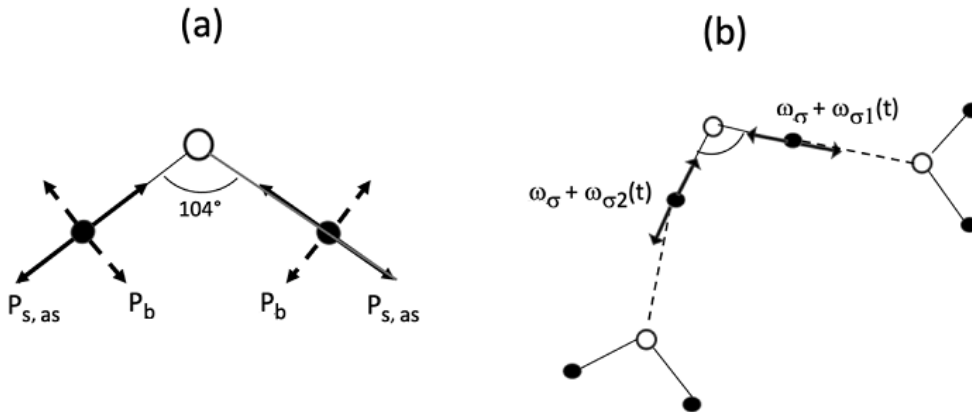


**Fig. 7.** (a) Vibrational modes in a free water molecule and (b) Stretching vibrations modified through hydrogen bonds.

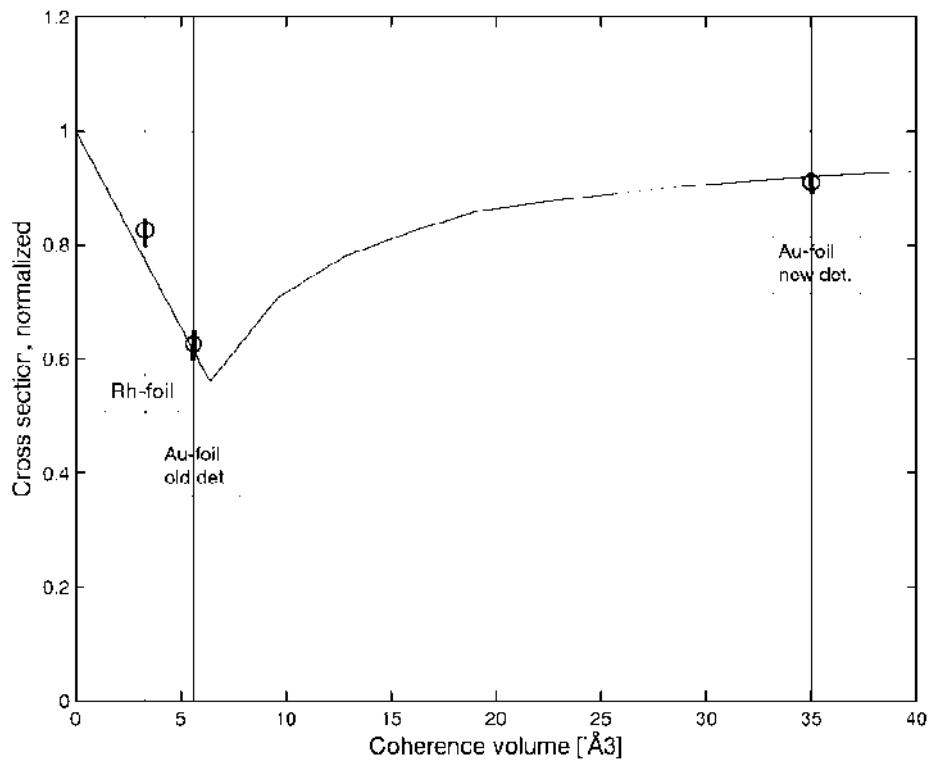


**Fig. 8.** Sketch of maximum cross-section reductions expected for different detection setups: ‘old’ with Rh-foil, ‘old’ with Au-foil, ‘new’ with Au-foil. Calculated for HH –distance 2.3 Å. (Reproduced with permission from Karlsson, E. B. 2021, *Physica Scripta*, 96, 025104). For experimental data, see ref. [10].

### 3.7. Compton scattering involving $N$ indistinguishable particles

The number of nuclei  $N$  seen by each neutron (or X-ray) in a scattering experiment is set by the coherence volume  $V_{\text{coh}}$  of the beam. Eq. (14) is valid for  $N = 2$ , which turned out to be a good approximation under the experimental conditions at the original settings of eVS neutron spectrometer at ISIS, UK [10].  $V_{\text{coh}}$  can be approximately expressed by the product  $(l_{\text{coh}})_{\parallel} \times (l_{\text{coh}})_{\perp}^2$  where  $(l_{\text{coh}})_{\parallel}$  is the longitudinal coherence length (set by the energy resolution of the beam) and  $(l_{\text{coh}})_{\perp}$  is the transverse coherence length (set by the detector geometry). Compton scattering experiments on metallic hydrides were later performed with reduced  $(l_{\text{coh}})_{\parallel}$  on eVS (giving  $N < 2$ ) and with increased  $V_{\text{coh}}$  on the modified VESUVIO spectrometer at UK [10], with coherence volumes covering up to  $N \approx 6$ .

Eq. (14) was extended in ref. [34] to  $N = 3$ , showing that entanglement of indistinguishable particles appears only pair-wise so that the reduction of the

cross-section for a  $N = 3$  system is only 2/3 of that for  $N = 2$  and in ref. [10] to  $N > 3$ . It was later understood that this phenomenon is a consequence of the general “entanglement monogamy” theorem [38] in quantum information theory. Fig. 8 above (from ref. [39]) illustrates the dependence on coherence volume  $V_{\text{coh}}$  for the effective neutron H-cross-section in metallic hydrides under three different experimental conditions and detector arrangements. The coherence length  $(l_{\text{coh}})_{\parallel}$  is set by the energy selection when the neutron passes resonance foils of Au-197 and Rh-103.

Similar scattering on selected small numbers of particles can hardly be realized by X-rays [39], but has been achieved with high energy electrons (see comments in [10, Section 7.2]).

## 4. Summary

Scattering on vibrating atoms has been of interest for more than 100 years, starting with Peter Debye [11] in 1913 and Ivar Waller [12] in 1923. Their

analyses became of outmost importance for the correct interpretation of X-ray (and later neutron) diffraction data, but left an open question whether zero energy terms should be taken into account.

For most atoms, zero-point vibrations are clearly visible in scattering only at low temperatures. At the end of the 1920s with data down to liquid nitrogen temperature (78 K), Waller and collaborators [14] could make conclusions about their existence, but only by comparing calculated and measured X-ray form factors for  $\text{Na}^+$  and  $\text{Cl}^-$  in NaCl. The actual deviation from linear T-dependence of the Debye-Waller factor at 78 K (indicating a zero-point contribution) was established in X-ray data from 1938 [16]. Clear evidence for zero-point contributions was later observed in neutron diffraction experiments, for instance on Mg-crystals [18], which could be extended to liquid He temperature (4 K).

Thermal neutron diffraction also enabled scattering experiments on low-Z elements, not easily accessible by X-ray diffraction. Their D-W factors are essentially larger and zero-point contributions are important already at room temperature. For hydrogen (H) it is the dominant contribution to the deviations  $\langle u^2 \rangle$  from equilibrium positions, but H-diffraction was limited with neutrons as well as with X-rays. With neutrons at epithermal energies, Compton scattering offered in the 1990s the possibility to map out the momentum distribution in detail [25] for particles in zero-point states (from which the corresponding spatial distribution  $n(x)$  can be derived).

Another striking effect of zero-point motion was first observed in 1997-99 in Compton scattering of neutrons on hydrogen-containing materials [29, 30], with settings such that each neutron sees only a limited number of protons ( $N = 2 - 6$ ). It was called the “hydrogen anomaly” because the neutron cross-sections appeared to be reduced by 20 – 40% compared to tabulated values. It lasted until 2012 before a full theoretical explanation [34] was proposed; it involved the notion of quantum entanglement enforced by the neutron’s interaction with two or more indistinguishable particles and the specific destructive interferences appearing when a neutron wave scatters on particles involved in zero-point motion. As shown in Section 3.6 the decay of the proton entanglement can be used to

study chemical processes on the lower femtosecond scale.

### CONFLICT OF INTEREST STATEMENT

There is no conflict of interest in the contents of this article.

### REFERENCES

1. Planck, M. 1901, *Annalen der Physik*. (Leipzig), 4(3), 553.
2. Planck, M. 1912, *Annalen der Physik* (Leipzig), 37, 642.
3. Landsberg, P. T. 1990, *Thermodynamics and Statistical Mechanics*, Courier Dover Publ.
4. Einstein, A. and Stern, O. 1913, *Annalen der Physik*, 345, 551.
5. Eucken, A. 1912, *Sitzungsber. der Königl. Preuss. Akad. der Wissensch*, 141 (unpublished)
6. Simon, F. 1934, *Nature*, 133, 529.
7. Lamb, W. and Retherford, R. 1947, *Phys. Rev.*, 72, 241.
8. Casimir, H. B. G. and Polder, D. 1948, *Phys. Rev.*, 73, 360.
9. Lamoreaux, S. K. 1997, *Phys. Rev. Lett.*, 78, 2.
10. Karlsson, E. B. 2018, *Physica Scripta*, 93, 035801.
11. Debye, P. 1913, *Annalen der Physik*, 348(1), 449.
12. Waller, I. 1923, *Zeitschrift für Physik A*, 17(1), 398.
13. Lipkin, H. 1961, *Phys. Rev.*, 123, 62.
14. James, R. W., Waller, I. and Hartree, D. R. 1928, *Proc. Roy. Soc. A*, 118, 334.
15. James, R. W. and Firth Miss 1927, *Proc. Roy. Soc. A*, 117, 62.
16. Brindley, G. W. and Ridley, P. 1938, *Proc. Phys. Soc.*, 50, 757.
17. Watanabe, Y., Iwasaki, H. and Ogawa, S. 1971, *Jap. J. Appl. Phys.*, 10, 786.
18. Sledziowska-Blocka, D. and Lebeck, B. 1976, *Acta Cryst. A*, 32, 150.
19. Gao, H. X., Peng, L.-M. and Zuo, J. M. 1999, *Acta Cryst. A*, 55, 1014.
20. Yang, Y. and Kawazoe, Y. 2012, *Europhysics Letters*, 98, 66007.
21. Wakabashi, N., Alefeld, B., Kehr, K. and Springer, T. 1974, *Solid State Comm.*, 15, 503.

22. Lovesey, S. W. 1987, *Theory of Neutron Scattering from Condensed Matter* (Oxford University Press, New York).
23. Andreani, C., Colognesi, D., Mayers, J., Reiter, G. F. and Senesi, R. 2005, *Advances in Physics*, 54(5), 377.
24. Reiter, G. F., Deb, A., Sakurai, Y., Itou, M., Krishnan, V. G. and Paddison, S. J. 2013, *Phys. Rev. Lett.*, 111, 036803.
25. Evans, A. C., Timms, D. N., Mayers, J. and Bennington, S. M. 1996, *Phys. Rev. B*, 53, 3023.
26. Squires, G. L. 1996, *Introduction to the Theory of Thermal Neutron Scattering*, Cambridge University Press.
27. Moreh, R. and Fogel, M. 1994, *Phys. Rev. B*, 50, 16184.
28. Warner, M., Lovesey, S. W. and Smith, J. 1983, *Z. Phys. B*, 51, 109.
29. Karlsson, E. B., Chatzidimitriou-Dreismann, C. A., Abdul-Redah, T., Streffer, R. M. F., Hjörvarsson, B., Öhrmalm, J. and Myers, J. 1999, *Europhys. Lett.*, 46, 617.
30. Chatzidimitriou-Dreismann, C. A., Abdul-Redah, T., Streffer, R. M. F. and Mayers, J. 1997, *Phys. Rev. Lett.*, 79, 2839.
31. Karlsson, E. B., Hartmann, O., Chatzidimitriou-Dreismann, C. A. and Abdul-Redah, T. 2016, *Meas. Sci. Technol.*, 27, 085501 [2017 Corrigendum.; 28 079501].
32. Watson, G. I. 1996, *J. Phys.: Condens. Matter*, 8, 5955.
33. Karlsson, E. B. and Lovesey S. W. 2000, *Phys. Rev. A*, 61, 062714.
34. Karlsson, E. B. 2012, *Int. J. Quant. Chem.*, 112, 587.
35. Mayers, J. and Abdul-Redah, T. 2005, in *Decoherence, Entanglement and Information Protection in Complex Quantum Systems*, NATO Science Series II Vol. 189, eds. V. M. Akulin, A. Sarfati, G. Kuritzki and S. Pellegrin (Springer, Dordrecht, 2005), 555-8; available at arXiv:quant-ph/0702038
36. Karlsson, E. B. 2003, *Phys. Rev. Lett.*, 90, 095301.
37. Bratos, S., Tarjus, G., Diraison, M. and Leicknam, J.-Cl. 1991, *Phys. Rev. A*, 44, 2745
38. Koashi, M. and Winter, A. 2004, *Phys. Rev. A*, 69, 022309.
39. Karlsson, E. B. 2021, *Physica Scripta*, 96, 025104.